ELSEVIER

Journal of Alloys and Compounds 313 (2000) 133–143

Journal of ALLOYS AND COMPOUNDS

www.elsevier.com/locate/jallcom

CVM calculation of the ternary system Co–Cu–Fe

S. Bein, C. Colinet*, M. Durand-Charre

Laboratoire de Thermodynamique et Physicochimie Métallurgiques, CNRS/INPG/UJF, ENSEEG, BP 75, F 38402 St. Martin d'Hères Cedex, France

Received 28 July 2000; accepted 15 August 2000

Abstract

The Co–Cu–Fe phase equilibria are calculated by means of the cluster variation method (CVM) in the temperature range 800–1000°C. For this purpose, the available experimental work on the ternary system Co–Cu–Fe, as well as on the three binary limiting systems, is reviewed. The interaction parameters involved in the thermodynamic model are fitted with a selected set of experimental data. The binary Fe–Cu, Cu–Co and Fe–Co diagrams are calculated and compared with the experimental ones. Several isothermal sections of the ternary system Co–Cu–Fe are calculated and compared with the experimental information. The evolution of the compositions of the three-phase equilibria with temperature is investigated in the ternary system.

Keywords: Transition metal alloys; Phase diagram; Thermodynamic modelling

1. Introduction

The only available experimental information concerning the Co–Cu–Fe phase diagram is from Jellinghaus [1] and Maddocks and Claussen [2] who proposed some vertical sections. Using these vertical sections and the limiting binary phase diagrams, approximate isothermal sections at 1000, 900 and 800°C have been constructed by Raghavan [3]. Concerning the Co–Cu–Fe phase diagram calculation, Hari-Kumar and Raghavan [4] have presented partial isothermal sections at 650, 750, 850 and 950°C calculated using the Calphad method. More recently Hari-Kumar and Wollants [5] performed thermodynamic calculations in the quaternary Co–Cu–Fe–Ni which include the ternary Co–Cu–Fe.

The purpose of the present work is to present results of calculations in the Co–Cu–Fe system. The modelling of binary or multicomponent phase diagrams may be performed by using the Calphad method. The models used involve phenomenological parameters which are fitted to the experimental information on the phase diagram and the thermochemical properties. Generally the excess Gibbs energy of mixing is expressed in the form of a standard Redlich Kister [6] polynomial, the ideal term being obtained from the sublattice model in the Bragg and Williams [7] approximation. However this method presents conceptual difficulties, in particular the short range order is not considered in the configurational entropy. In the present work we have used a mixed CVM-Calphad technique in which the configurational entropy is given by the cluster variation method (CVM). The input parameters are fitted on the available experimental data. In a first step the available experimental data found in literature for the limiting binaries and for the ternary were used to calculate isothermal sections at various temperatures. After this step, the experimental data were supplemented by new results from Durand-Charre and Mallet [8] in the ternary system and also in the limiting binaries Fe–Cu and Co–Cu. These new experimental determinations have been used to get a final set of values of the input parameters which has been used in the CVM calculation. The calculated isothermal sections are presented in this work.

The outline of this paper is as follows. In Section 2, we review some basic concepts of the CVM in fcc and bcc solid solutions. In Section 3, a critical assessment of the experimental phase diagrams data is presented. In Section 4 the values of the interaction parameters involved in our model, i.e. the interchange energies and the enhancement factors, obtained from the selected set of data, are provided. We present the calculated phase diagrams of the three binary subsystems and several calculated isothermal sections in the temperature range 800–1000°C. The results of the calculations are discussed with respect to ex-

*Corresponding author.

E-mail address: catherine.colinet@ltpcm.inpg.fr (C. Colinet).

0925-8388/00/$ – see front matter
PII: S0925-8388(00)01198-1

perimental ternary phase diagram data. Finally, Section 5 summarises our conclusions.

2. CVM in fcc and bcc solid solutions

2.1. Tetrahedron approximation of the CVM in fcc solid solutions

In fcc solid solutions, the simplest cluster is a regular tetrahedron including first nearest neighbor interactions. Descriptions of the tetrahedron approximation of the CVM in fcc solid solutions have been given in numerous papers for both binary and ternary solid solutions [9–11]. Hence, only a brief review of the calculations will be given here.

The three species Fe, Co, Cu occupying the lattice points are designated, respectively, by the index $i=1, 2, 3$. In the tetrahedron approximation, the configurational free energy is written in terms of the probability of having different arrangements of the point, the pair and the tetrahedron clusters. Such clusters probabilities will be designated by x_i, y_{ij}, and z_{ijkl} for the point, the pair and the tetrahedron, respectively, where the subscripts indicate the manner in which the clusters are populated by the three species (i,j,k,l each takes a value 1,2 or 3). In a system with N lattice points, the internal energy may be written as:

$$U_{\mathrm{fcc}} = 2N \sum_{i,j,k,l=1}^{3} e_{ijkl}\, z_{ijkl} \tag{1}$$

where $2N$ is the total number of tetrahedra and e_{ijkl} is the energy per tetrahedron in the i, j, k, l configuration. In the present instance we assume that only pairwise interactions ϵ_{ij} between first neighbours are predominant. Then the tetrahedron energy e_{ijkl} can be expressed in terms of these pairwise interactions according to:

$$e_{ijkl} = \frac{1}{2}(\epsilon_{ij} + \epsilon_{ik} + \epsilon_{il} + \epsilon_{jk} + \epsilon_{jl} + \epsilon_{kl}) \tag{2}$$

The factor $1/2$ is due to the fact that each pair is shared by two adjoining tetrahedra. It is common to take the energy of the pure components in the same structure as the alloy as the reference state. This reference energy is:

$$U^{0}_{\mathrm{fcc}} = N \sum_{i=1}^{3} 6\epsilon_{ii} x_i \tag{3}$$

With this reference state the internal energy can be rewritten in terms of the effective pair interactions $\Delta\epsilon_{ij} = \epsilon_{ij} - \frac{\epsilon_{ii} + \epsilon_{jj}}{2}$, the effective pair interactions are related to the so-called interchange energies by $W_{ij} = -2\Delta\epsilon_{ij}$. The expression of the internal energy is:

$$U_{\mathrm{fcc}} - U^{0}_{fcc} = 2N \sum_{i,j,k,l=1}^{3} \Delta e_{ijkl} z_{ijkl} \tag{4}$$

with:

$$\Delta e_{ijkl} = \frac{1}{2}(\Delta\epsilon_{ij} + \Delta\epsilon_{ik} + \Delta\epsilon_{il} + \Delta\epsilon_{jk} + \Delta\epsilon_{jl} + \Delta\epsilon_{kl}) \tag{5}$$

If such expression of the internal energy with composition independent effective pair interactions is used in a binary system, the thermodynamic data will be symmetric with respect to 0.5 composition. To break the symmetry, either composition dependent interchange energies or many-body interactions must be introduced. This last scheme, suggested by van Baal [12] and used later by Kikuchi et al. [10] for the calculation of ternary fcc systems, is carried out in the present work. The tetrahedron energy obtained by the sum of the pair interactions is multiplied by the proper enhancement factor. In each binary system there are two such factors whereas the total number of independent enhancement factors in ternary systems is nine. A general definition of the tetrahedron four body parameters designated by α_{ijkl} is given through the following relations for the tetrahedron energies:

$$\Delta e_{iiii} = 0 \tag{6a}$$

$$\Delta e_{iiij} = \frac{3}{2}\Delta\epsilon_{ij}(1 + \alpha_{iiij}) \qquad i \neq j \tag{6b}$$

$$\Delta e_{iijj} = 2\Delta\epsilon_{ij} \qquad i \neq j \tag{6c}$$

$$\Delta e_{iijk} = \left(\Delta\epsilon_{ij} + \Delta\epsilon_{ik} + \frac{1}{2}\Delta\epsilon_{jk}\right)(1 + \alpha_{iijk}) \qquad i \neq j \neq k \tag{6d}$$

Eq. 6a–d are valid for all values 1, 2 and 3, and permutations in e_{ijkl} of the subscripts i,j,k,l.

In the case of the fcc lattice Kikuchi [13] gave the expression of the configurational entropy using the regular tetrahedron as basic cluster. For a disordered fcc solid solution the configurational entropy is given by:

$$S_{\mathrm{fcc}} = Nk_{\mathrm{B}}\left[-2\sum_{i,j,k,l=1}^{3} L(z_{ijkl}) + 6\sum_{i,j=1}^{3} L(y_{ij}) - 5\sum_{i=1}^{3} L(x_i)\right] \tag{7}$$

with k_{B} the Boltzmann's constant and with the function $L(x)$ defined as: $L(x) = x \ln x$. In the model the free energy of mixing is given by:

$$\Delta_{\mathrm{mix}}F_{\mathrm{fcc}} = U_{\mathrm{fcc}} - U^{0}_{\mathrm{fcc}} - TS_{\mathrm{fcc}} \tag{8}$$

The reference state of the free energy of mixing is the pure constituents in the same structure let say here the fcc pure elements. If the chemical potentials of species i is derived from this equation, it will be referred to pure fcc i.

The equilibrium state of the system is derived by minimizing the grand potential Ω defined as:

$$\Omega = U - TS - N\sum_{i=1}^{3} \mu_i x_i \tag{9}$$

where μ_i are the chemical potentials of species i. Since we are not treating vacancies, the chemical potentials are not

all independent and we may introduce a new set of chemical potentials μ_i^* which fulfill the relation:

$$\sum_{i=1}^{3} \mu_i^* = 0 \tag{10}$$

It is easy to see that the new set of potentials, called the effective chemical potentials, is given by:

$$\mu_i^* = \mu_i - \frac{1}{3}(\mu_1 + \mu_2 + \mu_3) \tag{11}$$

The new grand potential, Ω^*, written as function of the effective chemical potentials is:

$$\Omega^* = U - TS - N\sum_{i=1}^{3} x_i \mu_i^* \tag{12}$$

Let us recall that the grand potential may also be expressed as function of the chemical potentials using:

$$\Omega^* = \frac{N}{3}\sum_{i=1}^{3} \mu_i \tag{13}$$

In the fcc solid solution we adopted as reference state of the thermodynamic data of mixing the pure fcc elements. The grand potential may also be referred to this reference state and will be written as:

$$\Omega^* = U_{\mathrm{fcc}} - U^0_{\mathrm{fcc}} - TS_{\mathrm{fcc}} - N\sum_{i=1}^{3} x_i \mu^*_{i,\mathrm{fcc}} \tag{14}$$

where the $\mu^*_{i,\mathrm{fcc}}$ are the effective chemical potential of species i referred to pure fcc constituents.

Combining Eqs. (4), (7) and (14), we obtain the CVM grand potential which must be minimized with respect to the cluster probabilities in order to yield the equilibrium state. Different minimization algorithms have been used with success in binary and ternary systems: the Newton–Raphson method and the natural iteration method (NIM) developed by Kikuchi [14]. In this work we have chosen the NIM to solve the minimisation equations which can be written:

$$z_{ijkl} = z^0_{ijkl} \exp\left(\frac{\lambda}{2Nk_{\mathrm{B}}T}\right) \tag{15}$$

with:

$$z^0_{ijkl} = Y^{\frac{1}{2}}_{ijkl} X^{-\frac{5}{8}}_{ijkl} \exp\left(\frac{-\Delta e_{ijkl}}{k_{\mathrm{B}}T}\right) \times \exp\left[\frac{\mu^*_{i,\mathrm{fcc}} + \mu^*_{j,\mathrm{fcc}} + \mu^*_{k,\mathrm{fcc}} + \mu^*_{l,\mathrm{fcc}}}{8Nk_{\mathrm{B}}T}\right] \tag{16}$$

$$Y_{ijkl} = y_{ij}y_{ik}y_{il}y_{jk}y_{jl}y_{kl}, \qquad X_{ijkl} = x_i x_j x_k x_l \tag{17}$$

λ is a Lagrange parameter introduced for the normalization of the tetrahedron probabilities:

$$\sum_{i,j,k,l=1}^{3} z_{ijkl} = 1 \tag{18}$$

The variables for subclusters are derived as linear combinations of the z_{ijkl}. For point variables one may write for example:

$$x_i = \sum_{j,k,l=1}^{3} z_{ijkl} \tag{19}$$

All the relations, which derive subcluster variables from the basic variables z, are called the reduction relations.

2.2. Tetrahedron approximation of the CVM in bcc solid solutions

Descriptions of the tetrahedron approximation of the CVM in bcc solid solutions have been given in various papers for both binary and ternary solid solutions [15–19]. The basic cluster is an irregular tetrahedron which edges made of two different lengths. The edges α–β and γ–δ are second neighbour bonds and the rest are first neighbour bonds.

The internal energy is usually written in terms of cluster interactions of the basic cluster, here tetrahedron interactions. Since in the bcc structure there are six tetrahedra per lattice point we may write:

$$U_{\mathrm{bcc}} = 6N\sum_{i,j,k,l=1}^{3} e_{ijkl} z_{ijkl} \tag{20}$$

If we assume that only pairwise interactions between first and second neighbours are dominant, the tetrahedron energy e_{ijkl} can be expressed as:

$$e_{ijkl} = \frac{1}{6}\left(\epsilon^{(1)}_{ik} + \epsilon^{(1)}_{il} + \epsilon^{(1)}_{jk} + \epsilon^{(1)}_{jl}\right) + \frac{1}{4}\left(\epsilon^{(2)}_{ij} + \epsilon^{(2)}_{kl}\right) \tag{21}$$

The fractions $1/6$ and $1/4$ take care of the fact that first and second neighbour bonds are shared with six and four tetrahedra, respectively. It is common use to take the energy of the pure components in the same structure as the alloy as reference. This reference energy is:

$$U^0_{\mathrm{bcc}} = N\sum_{i=1}^{3}\left(4\epsilon^{(1)}_{ii} + 3\epsilon^{(2)}_{ii}\right)x_i \tag{22}$$

With this reference state the internal energy can be rewritten in terms of the effective pair interactions, $\Delta\epsilon^{(k)}_{ij} = \epsilon^{(k)}_{ij} - \frac{\epsilon^{(k)}_{ii} + \epsilon^{(k)}_{jj}}{2}$, for $k=1$ and 2. The expression of the internal energy is:

$$U_{\mathrm{bcc}} - U^0_{\mathrm{bcc}} = 6N\sum_{i,j,k,l=1}^{3} \Delta e_{ijkl} z_{ijkl} \tag{23}$$

with:

$$\Delta e_{ijkl} = \frac{1}{6}\left(\Delta\epsilon^{(1)}_{ik} + \Delta\epsilon^{(1)}_{il} + \Delta\epsilon^{(1)}_{jk} + \Delta\epsilon^{(1)}_{jl}\right) + \frac{1}{4}\left(\Delta\epsilon^{(2)}_{ij} + \Delta\epsilon^{(2)}_{kl}\right) \tag{24}$$

As before for fcc solid solutions we have introduced tetrahedron four body interactions by multiplying the e_{ijkl}

by the proper enhancement factor. In a binary system there are three enhancement factors and in a ternary there are fifteen enhancement factors. A general definition of the four body tetrahedron interactions is given in the following equations:

$$\Delta e_{iiii} = 0 \tag{25a}$$

$$\Delta e_{iiij} = \left(\frac{1}{3}\Delta\epsilon_{ij}^{(1)} + \frac{1}{4}\Delta\epsilon_{ij}^{(2)}\right)(1+\alpha_{iiij}) \qquad i \neq j \tag{25b}$$

$$\Delta e_{iijj} = \frac{2}{3}\Delta\epsilon_{ij}^{(1)} \qquad i \neq j \tag{25c}$$

$$\Delta e_{ijij} = \left(\frac{1}{3}\Delta\epsilon_{ij}^{(1)} + \frac{1}{2}\Delta\epsilon_{ij}^{(2)}\right)(1+\alpha_{ijij}) \qquad i \neq j \tag{25d}$$

$$\Delta e_{iijk} = \left[\frac{1}{3}\left(\Delta\epsilon_{ij}^{(1)} + \Delta\epsilon_{ik}^{(1)}\right) + \frac{1}{4}\Delta\epsilon_{jk}^{(2)}\right](1+\alpha_{iijk}) \quad i \neq j \neq k \tag{25e}$$

$$\Delta e_{ijik} = \left[\frac{1}{6}\left(\Delta\epsilon_{ij}^{(1)} + \Delta\epsilon_{jk}^{(1)} + \Delta\epsilon_{ik}^{(1)}\right) + \frac{1}{4}\left(\Delta\epsilon_{ij}^{(2)} + \Delta\epsilon_{ik}^{(2)}\right)\right](1+\alpha_{ijik}) \qquad i \neq j \neq k \tag{25f}$$

These equations are valid for all values 1, 2 and 3 and permutations in Δe_{ijkl} of the subscripts i,j,k,l.

In the case of a bcc lattice, Kikuchi and Van Baal [15] were the first authors to give the expression of the configurational entropy. This expression is:

$$S_{\mathrm{bcc}} = Nk_{\mathrm{B}}\left[-6\sum_{i,j,k,l=1}^{3} L(z_{ijkl}) + 12\sum_{i,j,k=1}^{3} L(t_{ijk}) - 3\sum_{i,j=1}^{3} L\left(y_{ij}^{(2)}\right) - 4\sum_{i,k=1}^{3} L\left(y_{ik}^{(1)}\right) + \sum_{i=1}^{3} L(x_i)\right] \tag{26}$$

in the case of a disordered solid solution. The z_{ijkl}, t_{ijk}, $y_{ij}^{(2)}$, $y_{ik}^{(1)}$ and x_i are, respectively, the tetrahedron, triangle, second neighbour pair, first neighbour pair and point probabilities.

The equilibrium state is obtained by minimizing the grand potential defined as:

$$\Omega_{\mathrm{bcc}}^{*} = U_{\mathrm{bcc}} - U_{\mathrm{bcc}}^{0} - TS_{\mathrm{bcc}} - N\sum x_i\mu_{i,\mathrm{bcc}}^{*} \tag{27}$$

The choice of the reference state of the pure bcc elements implies that the grand potential and the effective chemical potentials are referred to the pure bcc elements. The minimization equations are:

$$z_{ijkl} = z_{ijkl}^{0}\exp\left(\frac{\lambda}{6Nk_{\mathrm{B}}T}\right) \tag{28}$$

with:

$$z_{ijkl}^{0} = T_{ijkl}^{\frac{1}{2}}U_{ijkl}^{-\frac{1}{4}}Y_{ijkl}^{-\frac{1}{6}}X_{ijkl}^{\frac{1}{24}}\exp\left(\frac{-\Delta e_{ijkl}}{k_{\mathrm{B}}T}\right) \times \exp\left[\frac{\mu_{i,\mathrm{bcc}}^{*} + \mu_{j,\mathrm{bcc}}^{*} + \mu_{k,\mathrm{bcc}}^{*} + \mu_{l,\mathrm{bcc}}^{*}}{24Nk_{\mathrm{B}}T}\right] \tag{29}$$

$$T_{ijkl} = t_{ijk}t_{ijl}t_{ikl}t_{jkl}, \qquad U_{ijkl} = y_{ij}^{(2)}y_{kl}^{(2)} \tag{30a}$$

$$Y_{ijkl} = y_{ik}^{(1)}y_{il}^{(1)}y_{jk}^{(1)}y_{jl}^{(1)}, \qquad X_{ijkl} = x_ix_jx_kx_l \tag{30b}$$

λ is a Lagrange parameter introduced for the normalization of the tetrahedron probabilities equation which is written the same as Eq. (18). The subcluster probabilities are related to the tetrahedron probabilities by using the reduction equations which could be written the same as Eq. (19).

2.3. Phase diagram calculation

Let us denote by φ_1 and φ_2 two phases possessing the same structure but having different compositions as it is the case when a phase separation phenomenon occurs. If we take μ_1^{*} and μ_2^{*} as independent potential variables in a ternary system, the phase boundary is obtained from the condition (temperature and volume fixed):

$$\Omega_{\varphi_1}^{*} = \Omega_{\varphi_2}^{*}, \quad \mu_{1,\varphi_1}^{*} = \mu_{1,\varphi_2}^{*}, \quad \mu_{2,\varphi_1}^{*} = \mu_{2,\varphi_2}^{*} \tag{31}$$

In the procedure of the phase diagram calculation, initial values are given to the effective chemical potentials, the grand potentials of the phases φ_1 and φ_2 are calculated, then the values of the chemical potentials are modified until the two grand potentials are equal.

In this work we will also treat the equilibrium between two phases having different structures, let us say fcc and bcc. In this case a common reference state of the chemical potential must be chosen. This common reference state corresponds to each pure element in a same structure R. $\mu_{i,\mathrm{R}}^{\mathrm{o}}$ are the chemical potentials of pure species i in this reference state. The equilibrium between the fcc and the bcc phases is obtained when the grand potentials of the fcc and bcc phases each referred to R are equal for same values of the effective chemical potentials. These of course are also referred to R. The relation between the effective chemical potentials and the effective chemical potentials are:

$$\mu_{i,\mathrm{R}}^{*} = (\mu_i - \mu_{i,\mathrm{R}}^{\mathrm{o}}) - \frac{1}{3}\sum_{i=1}^{3}(\mu_i - \mu_{i,\mathrm{R}}^{\mathrm{o}}) \tag{32}$$

To calculate the grand potential of either the fcc or the bcc phase using the relation (14) or (27), the effective chemical potentials must be referred either to fcc or to bcc. The connecting relations are:

$$\mu_{i,\mathrm{fcc}}^{*} = \mu_{i,\mathrm{R}}^{*} - (\mu_{i,\mathrm{fcc}}^{\mathrm{o}} - \mu_{i,\mathrm{R}}^{\mathrm{o}}) + \frac{1}{3}\sum_{i=1}^{3}(\mu_{i,\mathrm{fcc}}^{\mathrm{o}} - \mu_{i,\mathrm{R}}^{\mathrm{o}}) \tag{33}$$

$$\mu_{i,\mathrm{bcc}}^{*} = \mu_{i,\mathrm{R}}^{*} - (\mu_{i,\mathrm{bcc}}^{\mathrm{o}} - \mu_{i,\mathrm{R}}^{\mathrm{o}}) + \frac{1}{3}\sum_{i=1}^{3}(\mu_{i,\mathrm{bcc}}^{\mathrm{o}} - \mu_{i,\mathrm{R}}^{\mathrm{o}}) \tag{34}$$

Let us call $\Omega_{\mathrm{fcc}}^{*}$ the grand potential of the fcc phase referred to the pure elements in the fcc structure and $\Omega_{\mathrm{bcc}}^{*}$ the grand potential of the bcc phase referred to the pure elements in the bcc structure. These grand potentials must

be recalculated in a common reference state R, the connecting relations are:

$$\Omega^{*}_{\mathrm{fcc/R}} = \Omega^{*}_{\mathrm{fcc}} + \frac{1}{3}\sum_{i=1}^{3} x_i\left(\mu^{\mathrm{o}}_{i,\mathrm{fcc}} - \mu^{\mathrm{o}}_{i,\mathrm{R}}\right) \quad (35)$$

$$\Omega^{*}_{\mathrm{bcc/R}} = \Omega^{*}_{\mathrm{bcc}} + \frac{1}{3}\sum_{i=1}^{3} x_i\left(\mu^{\mathrm{o}}_{i,\mathrm{bcc}} - \mu^{\mathrm{o}}_{i,\mathrm{R}}\right) \quad (36)$$

As before the use of these relations needs the knowledge of the differences between the reference chemical potentials of the elements $\mu^{\mathrm{o}}_{i,\mathrm{fcc}} - \mu^{\mathrm{o}}_{i,\mathrm{R}}$ and $\mu^{\mathrm{o}}_{i,\mathrm{bcc}} - \mu^{\mathrm{o}}_{i,\mathrm{R}}$. These terms are the so-called lattice stabilities. The values of these thermodynamic data are found in the literature and also in compilations for example the SGTE compilation [20].

3. Selection of experimental and thermodynamic data

Since we have limited our calculations of isothermal sections of ternary diagram to the range 800–1000°C, the solubility limits determined by various authors are compared and discussed only in this temperature range.

As quoted above, in the course of the present study experimental data concerning the ternary Fe–Co–Cu as well as the two limiting binaries Fe–Cu and Co–Cu were performed by Durand-Charre and Mallet [8]. In this study the alloys were prepared from electrolytically pure iron and copper either by solid-state sintering (S) or by vacuum induction melting and casting (C). The samples were annealed for 40 days at 800°C, 10 days at 900°C and 5 days at 1000°C. The compositions were determined by microprobe analysis.

In the Cu–Fe, no mixing thermodynamic data were found in the solid state so the fit of interchange energies and enhancement factors (see Section 2) relies only on phase diagram data. In the Cu–Fe system, three solid-phases are identified: the fcc Cu-rich solid solution (γCu), the bcc Fe-rich solid solution α at low temperature and the fcc Fe-rich solid solution γ at high temperature. At 850°C the Cu–Fe phase diagram presents an eutectoid equilibrium $\gamma \leftrightarrow \alpha + (\gamma\mathrm{Cu})$. The solubility limits of both Cu in γ and α and Fe in (γCu) have been extensively measured and many references can be found in the literature. A complete review of the Cu–Fe system has been recently published by Swartzendruber [21]. Some of the most reliable values are reported in Fig. 1 [22–25]. The solubility limits reported from Durand Charre and Mallet [8] are close to the other experimental values. However, it seems that those latter values lead to an slightly higher solubility of iron in copper. In this last work the purity of the alloys was carefully checked because as it can be seen in the Fe–Co–O phase diagram [26] a very small amount of oxygen can drastically reduce the solubility of Cu in γ or α because of the formation of the FeO component.

The Co–Cu system has been reviewed by Nishizawa and Ishida [27]. The Co–Cu diagram presents in the solid-state, a large miscibility gap between the fcc Cu-rich solid solution (Cu) and the fcc Co-rich solid solution (γCo). The solubility limits were established by many authors [23,28–30]; they are displayed in Fig. 2. The recent measurements carried out by Durand-Charre and Mallet [8] using the same experimental procedure as for the Fe–Cu system provide values which are in very good agreement with the assessed ones. Let us quote that values of the cobalt activity have been provided by Dench and Kubaschewski [31] for compositions corresponding to the fcc miscibility gap.

The Fe–Co diagram has been recently reviewed by Nishizawa and Ishida [32], three phases are identified in

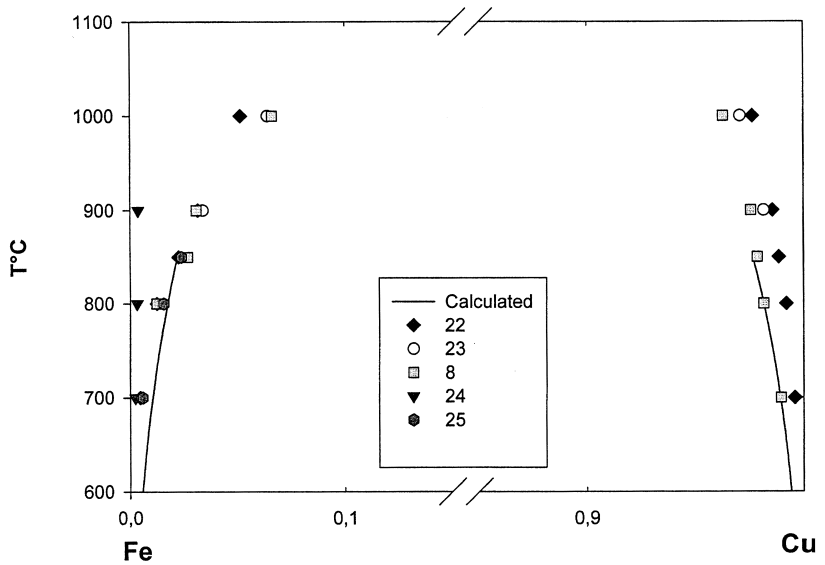

Fig. 1. Fe–Cu phase diagram.

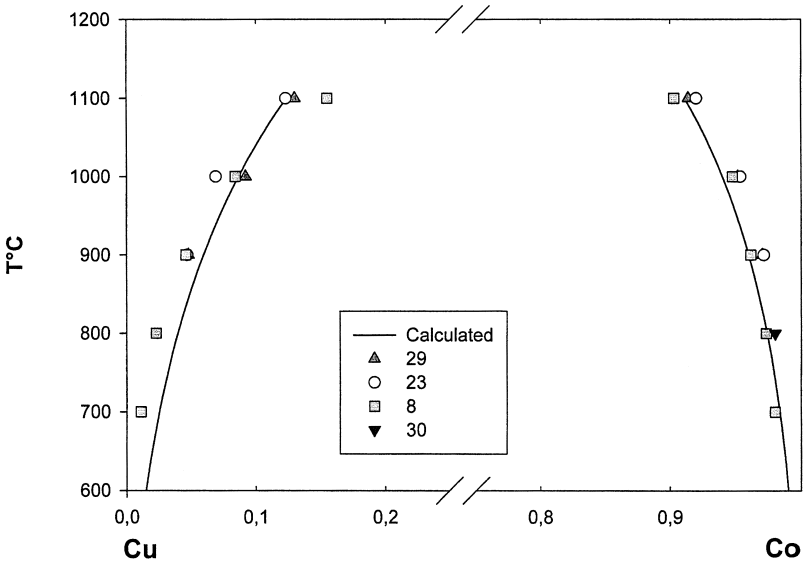

Fig. 2. Co–Cu phase diagram.

the solid state: the A2 bcc solid solution α, the A1 fcc solid solution γ and the ordered B2 bcc solid solution α′. The order/disorder transition is found at about 720°C and 48% of Co. Since the temperature range investigated in this paper is 800–1000°C, we will not consider the order/disorder transformation in the present work. Above 900°C and 50% iron, the α/γ boundary is well established since the measurements of several authors are in relatively good agreement [33–35] (Fig. 3). Below 900°C and for less than 30% iron, the assessed α/γ phase boundary [32] is based on the work of Ellis and Greiner [33] who took into account many previous papers (Fig. 3). However the α/γ phase boundary determined by Masumoto and Watanabe [35] is in disagreement with the later results [33]. Indeed, the two-phase α+γ region obtained by Masumoto and Watanabe [35] seems to be very narrow compared to the assessed one [33]. Durand-Charre and Mallet [8] performed experiments in ternary Co–Cu–Fe alloys containing a very small amount of copper and obtained the α/γ phase boundary in the cobalt rich domain. Their results confirm the phase boundary proposed by Ellis and Greiner [33]

Experimental information concerning the ternary Fe–Co–Cu is very scarce in the literature. In the works of Jellinghaus [1] and Maddocks and Claussen [2], vertical sections were established for various compositions. Raghavan [3] constructed isothermal sections (which he qualified approximate) at 1000, 900, and 800° using the experimental vertical sections and the limiting binary phase diagrams. The experimental data obtained by Durand-Charre and Mallet [8] are plotted in Fig. 4a,e,g. In the 1000°C isothermal section, a miscibility gap is ob-

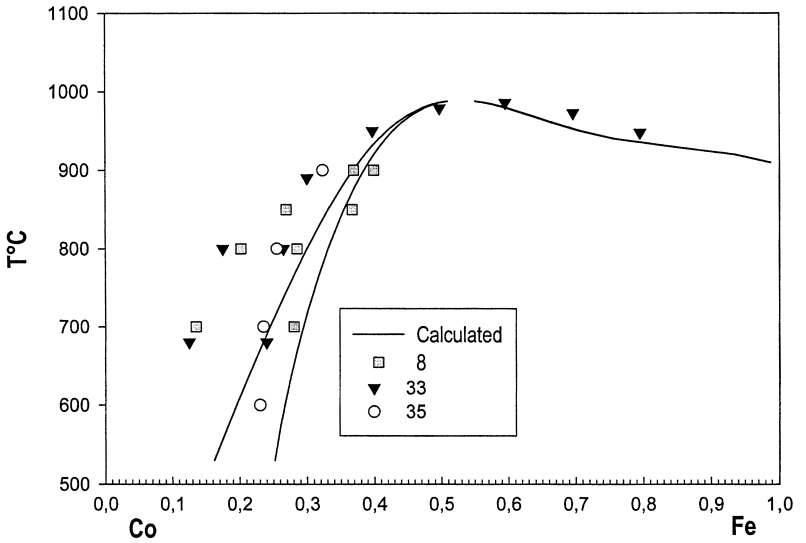

Fig. 3. Fe–Co phase diagram.

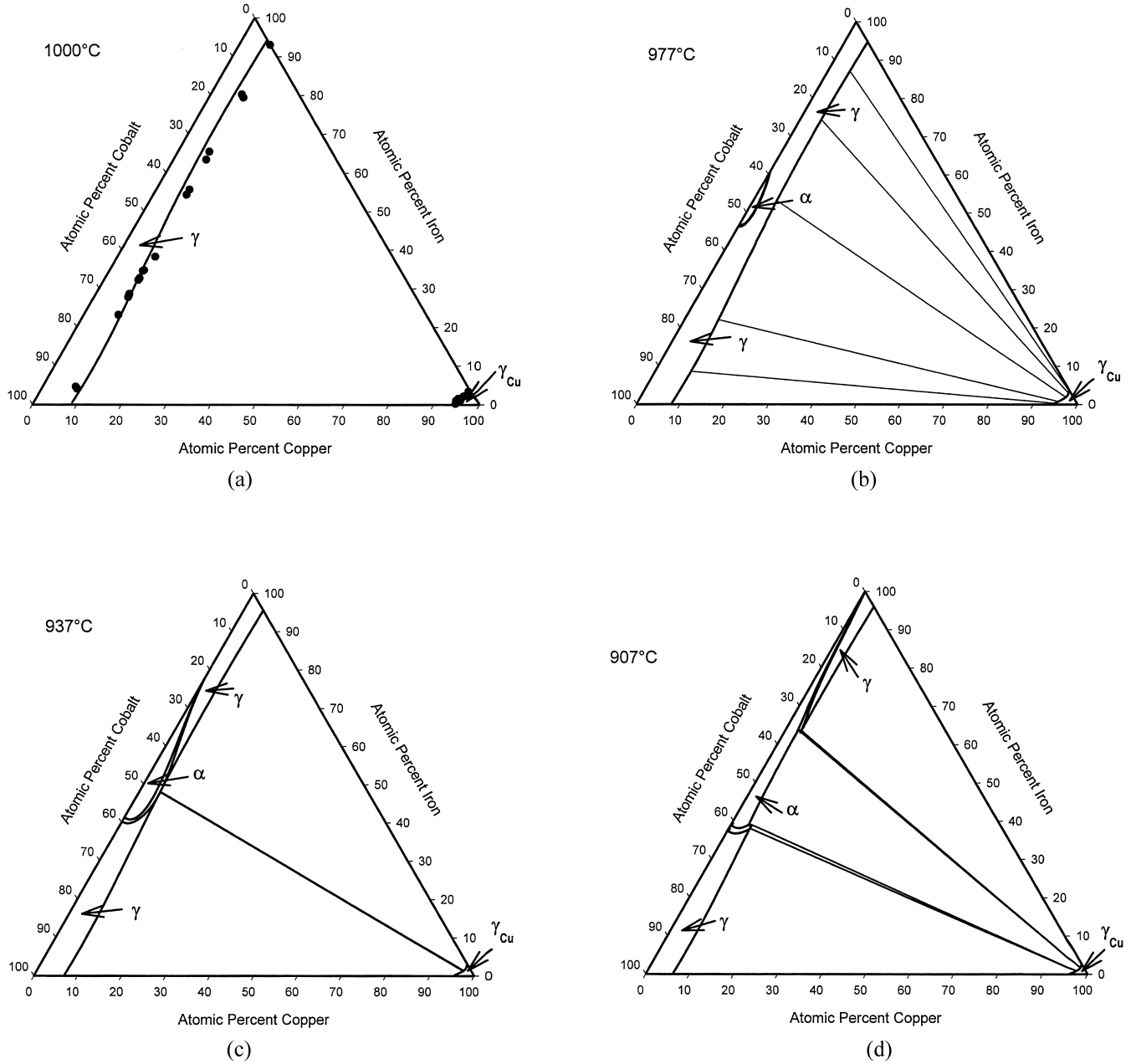

Fig. 4. Isothermal sections in the ternary Fe–Co–Cu. (a) $T=1000$°C, (b) $T=977$°C, (c) $T=937$°C, (d) $T=970$°C, (e) $T=900$°C, (f) $T=855$°C, (g) $T=800$°C. (—) Calculated phase boundaries, ● and ○ are experimental determinations from Durand-Charre and Mallet [8]. The full circles correspond to the compositions of the phases in equilibrium in the two-phase region. The open circles define the compositions of the phases in equilibrium in the three-phase region.

served between (γCu) and γ. In the 900°C isothermal section, three two phase regions (full circles) and two three-phases regions were detected by X-ray diffraction analysis. The three-phase regions are delimited by the open circles in Fig. 4. In the 800°C isothermal section one of the two-phase region has disappeared, and only one three-phase region between (γCu), γ, and α is detected.

As quoted before the phase diagram calculation between phases possessing different structures needs the knowledge of the lattice stability. For the Cu and Co components, the bcc form does not exist in nature, so the Gibbs energy difference between the bcc and fcc structures must be estimated. For Cu, the expression given by Jansson [36] and assessed in the review of Hari-Kumar and Raghavan [4] has been accepted in the present study. Concerning the lattice stability of bcc cobalt, large discrepancies are found in the literature (see the review of Fernandez-Guillermet [37]). The expressions of the free energy of the pure component assessed by Fernandez-Guillermet [37,38], have been adopted in SGTE data [20] and are used in the

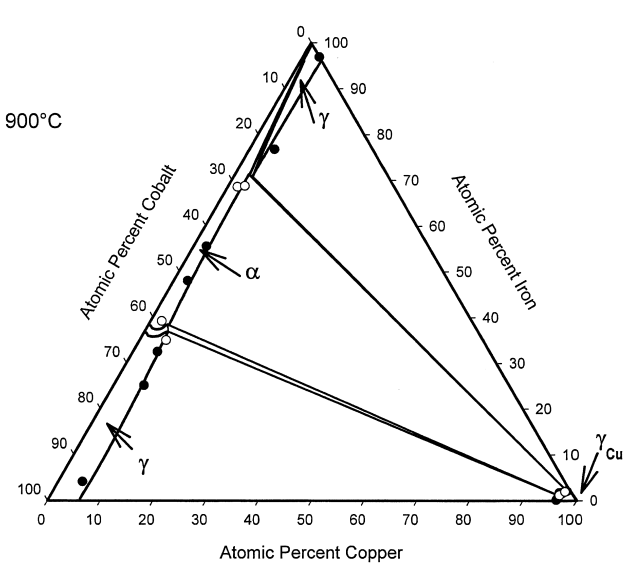

(e)

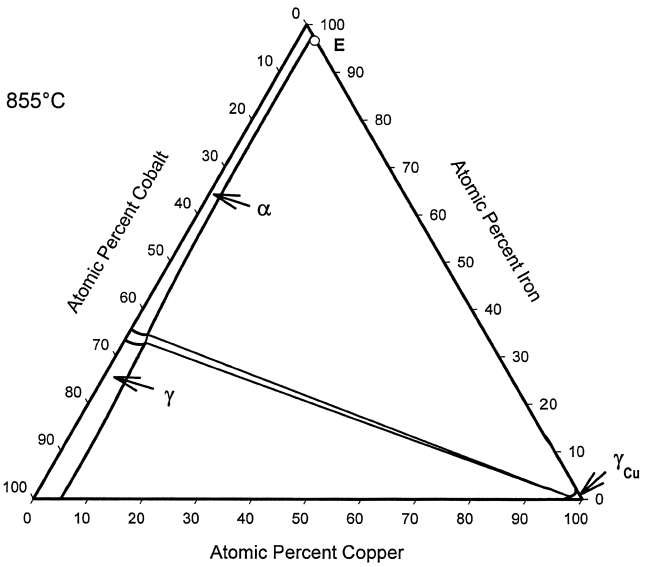

(f)

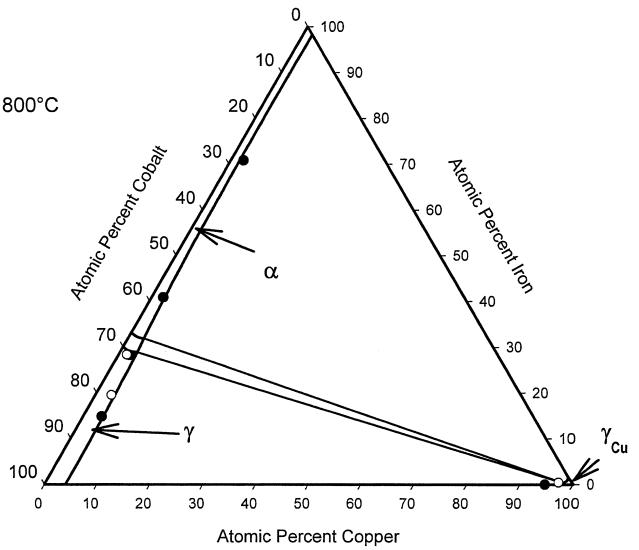

(g)

Fig. 4. (*continued*)

present work. The Fe Gibbs energy differences between the bcc and the fcc structures (both chemical and magnetic contributions) have been provided by Fernandez-Guillermet [39]. The overall expression is in excellent agreement with the curve displayed by Nishizawa [40]. For cobalt and for iron, the expressions of lattice stabilities used in this study include both chemical and magnetic terms. The magnetic interactions are not considered explicitly in the CVM calculation of the thermodynamic data for each phase because we just consider a three-component system, however they are taken into account in the lattice stability expressions and thus in the calculation of the phase equilibria.

4. Results and discussions

The selected experimental data available on the three limiting binary systems were used to fit the interchange energies and the enhancement factors in the binaries. All the ternary enhancement factors were taken equal to zero except the ternary enhancement factor $\alpha_{CuCuFeCo}$ which value was adjusted from the ternary phase diagram experimental data and more precisely on the shape of the phase boundary in the Cu corner. The fitted parameters are displayed in Table 1.

In the Cu–Fe system, the calculated phase boundaries are in good agreement with the experimental ones. The

Table 1
Interchange energies (J mol^{-1}) and enhancement factors

fcc phase		
Binary coefficients		
$W_{Cu,Fe} = -5850$ J mol^{-1}	$\alpha_{Cu,Cu,Cu,Fe} = 0.08$	$\alpha_{Fe,Fe,Fe,Cu} = 0.00$
$W_{Cu,Co} = -5400$ J mol^{-1}	$\alpha_{Cu,Cu,Cu,Co} = 0.10$	$\alpha_{Co,Co,Co,Cu} = -0.02$
$W_{Fe,Co} = 2485$ J mol^{-1}	$\alpha_{Fe,Fe,Fe,Co} = -0.02$	$\alpha_{Co,Co,Co,Fe} = -0.41$
Ternary coefficients		
$\alpha_{Cu,Cu,Fe,Co} = -0.40$	$\alpha_{Cu,Fe,Fe,Co} = 0.00$	$\alpha_{Cu,Fe,Co,Co} = 0.00$
bcc phase		
Binary coefficients		
$W^{(1)}_{Cu,Fe} = -8812$ J mol^{-1}	$W^{(2)}_{Cu\ Fe} = 0$ J mol^{-1}	
$W^{(1)}_{Cu,Co} = -6050$ J mol^{-1}	$W^{(2)}_{Cu\ Co} = 0$ J mol^{-1}	
$W^{(1)}_{Fe,Co} = 4157$ J mol^{-1}	$W^{(2)}_{Fe\ Co} = 0$ J mol^{-1}	
All α are equal to zero		
Ternary coefficients: all α are equal to zero		

eutectoid transformation $\gamma \leftrightarrow \alpha + (Cu)$ is correctly fitted considering the selected lattice stability of Fe [39]. The calculated eutectoid temperature 850°C is the same as the experimental one [21] while the compositions of the phases in at%Cu: 3.1% (γ), 2.2% (α) and 97.7% (γCu) are slightly higher than the assessed ones: 2.7% (γ), 1.9% (α) and 98.7% (γCu) but they agree with the selected set of experimental data [8].

In the Cu–Co system, the solubilities in (γCu)- and γ-phase are a little higher than in the Cu–Fe system, thus the interchange energy is a little lower (-5400 instead of -5850 J). This value, as well as the values of enhancement factors, is derived from the experimental results of Durand-Charre and Mallet [8]. The calculated phase boundaries fall within the selected experimental ones. Moreover the calculated values of the cobalt activity are in good agreement with the experimental values obtained by Dench [31]

The interchange energy value of the bcc Fe–Co solid solution $W^{(1)}_{Fe\ Co} = 4157$ J, $W^{(2)}_{Fe\ Co} = 0$ assessed by Inden [41] has been taken in the present paper. Moreover, with the same value and by taking into account the magnetic interactions, Colinet et al. [19] determined the correct B2→A2 order–disorder transformation temperatures of the Fe–Co system. With the selected lattice stabilities of Fe and Co, the optimization of the interchange energy and the dissymmetry coefficients of the fcc Fe–Co solid solution leads to the calculated phase boundaries displayed in Fig. 3. The agreement is quite good for less than 60% Co and above 900°C. The temperature of the maximum of the $\alpha + \gamma$ phase boundary is found at 988°C and 52% at Fe whereas the experimental temperature is 985°C at 54%. However in the Co-rich region of the phase diagram, the calculated $\alpha + \gamma$ field is narrower than the experimental assessed one [32], and the Co concentration at the phase boundary is too low compared to the measurements. In order to improve the agreement between calculated and experimental $\gamma/\alpha + \gamma$ and $\alpha/\alpha + \gamma$ phase boundaries, tentative calculations were performed with different expression of lattice stabilities. Most of the lattice stability values of Co proposed in the literature [42–44,4] (here, the lattice stability is the Gibbs energy difference between the bcc and the fcc structure) are higher than the assessed one and decrease with increasing temperature in the temperature range where the α/γ transformation occurs. This might lead to a wrong diagram since no maximum temperature of the α/γ equilibrium was obtained with the expression of [4]. In addition, the lattice stability values of Fe are very small (less than 200 J mol^{-1}) between the two transition temperatures of Fe and a little change in these values induces drastic changes in the positions of phase boundaries. Slightly higher values would fairly improve the accordance with experimental results. This strong dependence of the α/γ boundaries positions with respect to the lattice stabilities of Fe and Co is related to the very similar plots of the free energies of bcc and fcc Fe–Co alloy versus composition [40].

Being aware of the difference between the calculated and the experimental Fe–Co α/γ boundaries (Fig. 3), isothermal sections of the ternary Fe–Co–Cu system have been calculated at 1000, 977, 937, 907, 900, 855, 800°C and are reported in Figs. 4a–g. Experimental information about the Fe–Co–Cu system is available at 1000, 900, and 800°C [8]. These experimental values are marked by open and full circles on isothermal sections presented in Fig. 4. Thus, the comparison can be drawn at these temperatures between experimental and calculated results. In addition, several other isothermal sections were calculated in order to study the effect of temperature on the position of phase boundaries and critical tie-lines.

At 1000°C, the calculated phase diagram (Fig. 4a) shows a miscibility gap between the fcc Cu-rich solid solution (γCu) and the fcc Fe–Co rich solid-solution (γ). The calculated phase boundaries are in agreement with limiting

binary values and with the experimental value on ternary alloy. The phase boundary located in the Cu-rich corner of the isothermal section exhibits a pronounced curvature even if the ternary enhancement factors are equal to zero. This should be related to the ordering tendency of the equiatomic Fe–Co which would enhance the phase separation between the Cu-rich solid solution on one hand and the Fe–Co rich solid solution on the other one.

When the temperature decreases from 1000°C, an α-field emerges from the Fe–Co edge at the calculated temperature (988°C) of the maximum of α-phase stability in the Fe–Co binary diagram and at the corresponding composition (about 52% Fe). It develops into the ternary diagram at lower temperatures in half-cone shape, surrounded by a thin $\alpha+\gamma$ field (see Fig. 4b at 977°C). At the same time, the miscibility gap between (Cu) and γ-phase increases its extent with decreasing temperature. Therefore, at 937°C (Fig. 4c), the $\gamma/\alpha+\gamma$ phase boundary intersects the $\gamma/(\gamma Cu)+\gamma$ phase boundary at 4.75% at Cu and 48.1% at Fe. At this intersection point, the three phases $\alpha+\gamma+(\gamma Cu)$ are in equilibrium. When the temperature decreases, this critical tie-line gives rise to two three-phase fields equilibria and two distinct thin $\alpha+\gamma$ fields. At the same time, the $\alpha/(\gamma Cu)+\alpha$ boundary extends. The intersection of both these $\alpha+\gamma$ two-phase regions with the Fe–Co edge move from each other and at 907°C (the calculated α/γ transition temperature of Fe), one of them reaches the Fe-corner as seen in Fig. 4d. Then, between 907 and 850°C, the corresponding $\alpha+\gamma$ field intersects the Fe–Cu edge since an $\alpha+\gamma$ region is found in the binary Fe–Cu in this temperature range.

At 900°C (Fig. 4e), the positions of the two three-phase equilibria are consistent with the experimental results [8]. The calculated solubility limits of Cu are lower in the α-phase than in the γ-phase and are in good agreement with the measurements [8].

At 855°C, one of the two three-phase triangles is identical to the Fe–Cu edge (Fig. 4). Then, this flat triangle represents the eutectoid equilibrium $\gamma\leftrightarrow\alpha+(\gamma Cu)$ in the Fe–Cu system. The eutectoid composition of the γ-phase is marked by an open circle on the 855°C isothermal section. Below 855°C, this three-phase equilibrium disappears whereas the other three-phase region remains. Therefore, the isothermal section is divided into two main parts: an $\alpha+(\gamma Cu)$ two phase-field for higher Fe content and a $\gamma+(\gamma Cu)$ two phase-field for higher Co content.

In the 800°C isothermal section (Fig. 4f), the position of the three-phase equilibria: α, γ, and (γCu) is not correctly represented, this is certainly due to the inability of our model to fit accurately the experimental α/γ phase boundary in the Co rich part of the Fe–Co diagram. The calculated solubilities of Cu in the α- and γ-phase are quite similar and are in accordance with experimental results. In the Cu-rich corner, a discrepancy is observed between the results of calculations and measurements. We suppose the measured solubilities are too high. Indeed, the Cu-interdendritic regions are often too narrow to avoid completely the presence of the Fe and Co rich α- or γ-phase in microprobe analysis volume. Moreover, since the analysed (Cu)-phase is nearly pure at this temperature, a very small amount of the Fe and Co rich phase could induce drastic discrepancies in the measured composition.

Calculations of additive isothermal sections at lower temperature show that the ternary diagram keeps the same shape with diminishing solubilities.

The eutectoid invariant equilibrium $\gamma\leftrightarrow\alpha+(\gamma Cu)$ in the Fe–Cu system becomes a curve in the ternary system. This curve originates from the Fe–Cu edge at the eutectoid temperature 855°C and raises to a limit point at 937°C in the ternary diagram. Because of the γ/α transformation in the Fe–Co system, a second $\gamma/\gamma+\alpha$ boundary originates from the Fe–Co edge. The curve defined, like the eutectoid curve, by the intersection between this phase boundary and the $\gamma/\gamma+(Cu)$ boundary meets the eutectoid curve at the limit point.

5. Conclusion

The thermodynamic calculation of the ternary diagram Fe–Co–Cu was achieved in the temperature range 800–1000°C. A phase separation is always observed in the ternary system between the Cu-rich phase and the Fe and Co-rich ones. The Fe and Co-rich phase is fcc at high temperature (γ). Below 988°C, a bcc Fe and Co-rich solution (α) becomes also stable near the equiatomic composition. The corresponding bcc field expands in the ternary diagram giving rise to two narrow three-phase fields. At 855°C, one of them is identical to the Fe–Cu edge: this corresponds to the eutectoid equilibrium. Below 855°C, only one three-phase field remains: the Fe-rich phase is bcc (α) whereas the Co-rich phase is fcc (γ).

The calculated binary diagrams and the calculated isothermal sections are, for the major part, in good agreement with the experimental phase diagrams data. The Fe–Co–Cu phase diagram has been deeply revisited and modified compared to the one published by Raghavan [3]. However, the calculation of the γ/α phase boundaries in the binary Fe–Co diagram as well as in the ternary diagram has to be improved in order to fit better the experimental data. For this purpose, in further studies, the magnetic components Fe^{+} Fe^{-} Co^{+} Co^{-} will be treated separately in the CVM.

References

[1] W. Jellinghaus, Arch. Eisenhuttenwes. 3 (1936) 10.
[2] W.R. Maddocks, G.E. Claussen, Iron Steel Inst. Spec. Rep. 14 (1936) 116.

[3] V. Raghavan, in: Phase Diagrams of Ternary Iron Alloys, Vol. 6A, Indian Institute of Metals, Calcutta, 1992, p. 597.
[4] K.C. Hari Kumar, V. Raghavan, J. Alloy. Phase Diag. 5 (1989) 201.
[5] K.C. Hari Kumar, P. Wollants, Calphad 28 (1999) 94.
[6] O. Redlich, A. Kister, Ind. Eng. Chem. 40 (1948) 345.
[7] W.L. Bragg, E.J. Williams, Proc. R. Soc. (Lond.) A145 (1934) 699.
[8] M. Durand-Charre, S. Mallet, Unpublished research, ENSEEG (LTPCM), France.
[9] R. Kikuchi, Acta Metall. 25 (1977) 195.
[10] R. Kikuchi, D. de Fontaine, Acta Metall. 25 (1977) 207.
[11] R. Kikuchi, J.M. Sanchez, D. de Fontaine, H. Yamauchi, Acta Metall. 28 (1980) 651.
[12] C.M. van Baal, Physica 64 (1973) 571.
[13] R. Kikuchi, Phys. Rev. 81 (1951) 988.
[14] R. Kikuchi, J. Chem. Phys. 60 (1974) 1071.
[15] R. Kikuchi, C.M. van Baal, Scripta Metall. 8 (1974) 425.
[16] N.S. Golosov, A.M. Tolstik, J. Phys. Chem. Solids 36 (1975) 899.
[17] N.S. Golosov, A.M. Tolstik, J. Phys. Chem. Solids 36 (1975) 903.
[18] H. Ackermann, G. Inden, R. Kikuchi, Acta. Metall. 37 (1989) 1.
[19] C. Colinet, G. Inden, R. Kikuchi, Acta. Metall. Mater. 41 (1993) 1109.
[20] A.T. Dinsdale, Calphad 15 (1991) 317.
[21] L.J. Swartzendruber (Ed.), Phase Diagrams of Binary Iron Alloys, ASM International, Washington, DC, 1993, p. 131.
[22] G. Salje, M. Feller-Kniepmeier, Z. Metallkd. 63 (1978) 167.
[23] M. Hasebe, T. Nishizawa, Calphad 4 (1980) 83.
[24] E.P. Abrahamson II, S.L. Lopata, Trans. Metall. Soc. AIME 236 (1966) 76.
[25] H.A. Wriedt, L.S. Darken, Trans. Metall. Soc. AIME 218 (1960) 30.
[26] V. Raghavan (Ed.), Phase Diagrams of Ternary Iron alloys, The Indian Institute of Metals, Calcutta, 1989, p. 105, Part 5.
[27] T. Nishizawa, K. Ishida, Bull. Alloy Phase Diag. 5 (1984) 161.
[28] F.J. Bruni, J.W. Christian, Mater. Sci. Eng. 9 (1972) 241.
[29] C.F. Old, C.W. Haworth, J. Inst. Metals 94 (1966) 303.
[30] J.D. Livingston, Trans. Met. Soc. AIME 215 (1959) 566.
[31] W.A. Dench, O. Kubaschewski, High Temp. High Press. 1 (1969) 357.
[32] T. Nishizawa, K. Ishida (Eds.), Phase Diagrams of Binary Iron Alloys, ASM International, Washington, DC, 1993, p. 93.
[33] W.C. Ellis, E.S. Greiner, Trans. ASM 29 (1941) 415.
[34] A.S. Normanton, P.E. Bloomfield, F.R. Sale, B.B. Argent, Met. Sci. 9 (1975) 510.
[35] H. Masumoto, K. Watanabe, Sci. Rep. Res. Inst. Elect. Magn. Alloys 127 (1979) 1.
[36] A. Jansson, Report TRITAMAC-0340, Royal Institute of Technology, Stockholm, Sweden, 1987.
[37] A.F. Guillermet, High Temp. High Press. 19 (1987) 477.
[38] A.F. Guillermet, Int. J. Thermophys. 6 (1987) 481.
[39] A.F. Guillermet, High Temp. High Press. 19 (1987) 477.
[40] T. Nishizawa, J. Phase Equilibria 16 (1995) 379.
[41] G. Inden, Z. Metallkd. 66 (1977) 529.
[42] L. Kaufman, H. Nesor, Z. Metallkd. 64 (1973) 249.
[43] N. Saunders, P. Miodownik, Metastable lattice stabilities for the elements, Department of Material Science and Engineering, University of Surrey, Guilford, Surrey, GU25XH, UK, 1986.
[44] P. Miodownik (Ed.), Chemical Metallurgy of Iron and Steel, The Iron and Steel Institute, London, 1973, p. 292.